Available online at www.sciencedirect.com
SCIENCE DIRECT®
ELSEVIER
International Journal of Solids and Structures 42 (2005) 3716–3729
INTERNATIONAL JOURNAL OF SOLIDS and STRUCTURES
www.elsevier.com/locate/ijsolstr

Unloading of an elastic–plastic loaded spherical contact

I. Etsion *, Y. Kligerman, Y. Kadin

Department of Mechanical Engineering, Technion—Israel Institute of Technology, Technion City, 32000 Haifa, Israel

Received 7 October 2004; received in revised form 5 December 2004
Available online 21 January 2005

Abstract

The process of unloading of an elastic–plastic loaded sphere in contact with a rigid flat is studied by finite element method. The sphere material is assumed isotropic with elastic-linear hardening. The numerical simulations cover a wide range of material properties and sphere radius. The contact load, stresses, and deformation in the sphere during both loading and unloading, are calculated for a wide range of interferences. Analytical dimensionless expressions are presented for the unloading load–deformation relation, the residual interference and the residual curvature of the sphere after complete unloading. A new measure termed elastic–plastic loading index is introduced to indicate the plasticity level of the loaded sphere. Some ideas regarding reversibility of the unloading process and elasticity of multiple loading unloading are also presented.

Keywords: Spherical contact; Elastic–plastic contact; Load–Unload

1. Introduction

Repeated loading and unloading of rough surfaces is an important problem, especially in the technology of micro/nano-systems, such as MEMS microswitches (Majumder et al., 2001, 2003), for example, or head–disk interaction (Peng and Bhushan, 2003) in magnetic storage system. Hence, the interest in loading/unloading of a sphere in contact with a flat, which can simulate a single asperity of a rough surface, is obvious.

Johnson (1985) offered one of the first simple analytical models of unloading an elastic plastic spherical indentation contact. Johnson claimed that even though large plastic deformations can occur during

* Corresponding author. Tel.: +972 4 829 2096; fax: +972 4 829 5711.
E-mail address: etsion@tx.technion.ac.il (I. Etsion).

0020-7683/$ - see front matter © 2004 Elsevier Ltd. All rights reserved.
doi:10.1016/j.ijsolstr.2004.12.006

Nomenclature

a	contact radius
A	real contact area
A_c	real contact area at the inception of plastic deformation
A_{max}	real contact area before unloading
A^*	dimensionless contact area, A/A_c
E	Young's modulus
E^*	Hertz elastic modulus
H	hardness of the sphere
K	hardness factor, $0.454 + 0.41\nu$
p_0	maximum pressure at the contact center
P	contact load
P_c	contact load at the inception of plastic deformation
P_{max}	maximum contact load before unloading
P^*	dimensionless contact load, P/P_c
r	radial coordinate
R	original sphere radius
R_{res}	residual central curvature after complete unloading
u_z	axial displacement
ν	Poisson ratio
σ_y	yield stress in tension
ω	contact interference
ω_c	critical interference at the inception of plastic deformation
ω_{max}	maximum contact interference before unloading
ω_{res}	residual contact interference after complete unloading
ω^*	dimensionless interference, ω/ω_c

loading, it is intuitive to expect the unloading process to be perfectly elastic. Johnson justified this hypothesis based on Tabor (1948) observations of spherical indentation for hardness measurement.

Mesarovic and Johnson (2000) examined the process of unloading of two elastic–plastic spheres following very large indentation which made their contact fully plastic with a uniform contact pressure distribution. It was assumed that during unloading to the point of pull-off, the deformation is predominantly elastic. Hence, while the loading process was solved numerically the unloading solution was analytical.

Vu-Quoc et al. (2000) presented a simplified analytical load–unload model for the normal force–displacement relation in elastic–plastic contacting spherical particles. The authors compared their model with a nonlinear finite element model involving plastic flow in both loading and unloading conditions and found good agreement. This model however was limited to relatively small normal loads, which, in the specific dimensional case presented in the paper, amounts to interferences less than eight times that of the critical one at yielding inception.

A study of the time dependent adhesive load–unload of viscoelastic material spheres was carried out by Lin and Hui (2002) using finite element simulation. Upon reaching a maximum load, the spheres were unloaded until complete separation. The authors studied the effect of loading and unloading rates on hysteresis and the pull-off force.

Yan and Li (2003) presented a numerical study of the cyclic indentation of an elastic–perfectly plastic half space by a rigid sphere using a nonlinear finite element method. Results of the contact pressure

distribution, force–displacement relationship, and contact radius during loading and unloading were presented in a dimensionless form for steel flat. The authors found that subsequent load–unload cycles following the first unloading are perfectly elastic but do not obey the Hertz theory.

Ye and Komvopoulos (2003) studied the effect of residual stresses on contact deformation of elastic–plastic layered media. Two different loading types were analyzed: (a) normal contact consisting of indentation loading and unloading, and (b) sliding contact consisting of indentation, sliding and full unloading. A three-dimensional finite element model of a rigid sphere interacting with a deformable layered medium was developed. It was shown that the optimum residual stress which results in the lowest equivalent stress in the surface layer upon subsequent loading depends on the type of contact loading, coefficient of friction, and dominant deformation mode (plastic deformation or cracking) in the layer.

Li et al. (2002) presented a theoretical load–unload model for the frictionless contact of a rigid sphere with an elastic–perfectly plastic half-space or an elastic–perfectly plastic sphere with a rigid flat. Formulae describing the force–displacement relationship for static contact problems were derived. This model can be considered a modification of Johnson's (1985) and Vu-Quoc et al. (2000) models by using a better approximation of the contact pressure distribution function, and considering the variation in the curvature of the contact surface during the contact interaction. The theoretical results compared favorably with FEA results for a typical steel half space.

Kim et al. (2004) performed ultrasonic experiments to characterize the elasto-plastic contact between two rough surfaces. The experiments were performed by cyclic loading and unloading taking into account the effect of hysteresis. The frequency-dependent ultrasonic reflection coefficient from the interface was measured during loading and unloading cycles as function of the applied pressure.

As can be seen from the above literature review a complete universal solution for the unloading of an elastic–plastic sphere is still missing. The main goal of the present paper is to develop a model for the unloading of an elastic–plastic loaded sphere in a frictionless contact with a rigid flat. This is also equivalent to the interaction between two identical spheres having the same radius and physical properties. Since a spherical contact may also simulate a single asperity of a rough surface the present analysis can also help understand the behavior of rough surfaces during repeated loading and unloading.

2. The unloaded spherical contact model

A schematic representation of the contact problem is shown in Fig. 1. A compliant hemispherical body of an original un-deformed radius R comes into contact with a rigid flat surface. The material of the sphere is assumed an elastic linear hardening, ductile isotropic material, with identical behavior in tension and compression.

The dashed and solid horizontal lines in Fig. 1 show the rigid flat positions before and after loading, respectively. The displacement, ω, of the rigid flat (which will be termed "interference" in the following), and the contact area with a radius, a, (see Fig. 1) correspond to a normal load, P, applied to the contact.

We assume that the contact interference, ω, is much smaller than the un-deformed sphere radius, R, but larger than the critical interference ω_c at the inception of plastic deformation (Chang et al., 1987). The contact radius, a, is also very small compared to R. Hence, the analysis is carried out assuming small strain theory.

The problem is axisymmetric (2D) about the z-axis. Therefore, for the complete analysis it is sufficient to consider only one half of the axisymmetric hemisphere section. The boundary conditions consist of constrain in the vertical direction at the hemisphere base and in the radial direction at its z-axis. Restricting also radial deformations at the hemisphere base does not affect the results of the analysis since this boundary is very far away and therefore has very little effect on the contact zone (see Kogut and Etsion, 2002).

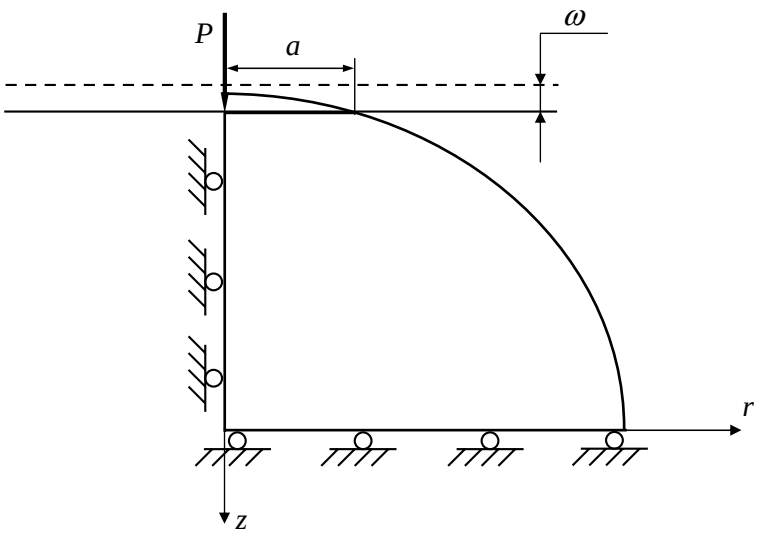

Fig. 1. Schematic model of the contact problem.

The spherical surface is free elsewhere except from the axial constriction enforced by the contacting rigid flat. The contact is assumed frictionless (perfect slip condition). Such a perfect slip condition between an elastic–plastic hemisphere and a rigid flat also simulate the contact condition between two identical spheres regardless of the friction between them.

The critical interference, ω_c, which causes plastic yield inception is given by:

$$\omega_c = \left(\frac{\pi K H}{2E^*}\right)^2 R \tag{1}$$

where the hardness, H, of the sphere is related to its yield stress by $H = 2.8\sigma_y$ (see Tabor, 1951); the hardness coefficient, K, is related to the Poisson ratio, v, of the sphere by (e.g., Chang et al., 1988) $K = 0.454 + 0.41v$; and E^* (the Hertz elastic modulus) is defined as:

$$\frac{1}{E^*} = \frac{1 - v_1^2}{E_1} + \frac{1 - v_2^2}{E_2} \tag{2}$$

where E_1, E_2 and v_1, v_2 are the Young moduli and Poisson ratios of the two materials in contact, respectively. In the case of a rigid flat $E_2 \to \infty$; and for a sphere material with $E_1 = E$; $v_1 = v$, the Hertz elastic modulus is reduced to:

$$E^* = \frac{E}{1 - v^2} \tag{3}$$

While the elastic contact problem of a sphere and a rigid flat has an analytical solution (the classical Hertz solution, see e.g., Johnson, 1985; Timoshenko and Goodier, 1970), the elastic–plastic contact problem requires a numerical solution. In the present work this problem is solved using the approach of Kogut and Etsion (2002) for a frictionless contact between an elastic–perfectly plastic sphere and a rigid smooth flat.

The solution consists of two stages. In the first one the sphere is loaded by the rigid flat to a dimensionless interference $\omega^* = \omega/\omega_c$. During this stage the interference ω is gradually increased up to a desired maximum value, ω_{max}, and the contact load, the contact radius and the real contact area, reach their maximum

values P_{max}, a_{max} and A_{max} respectively. The dimensionless contact load P/P_c, and contact area A/A_c as functions of the dimensionless interference $\omega^* = \omega/\omega_c$ during the elastic–plastic loading stage were given by Kogut and Etsion (2002) in the form:

$$\frac{P}{P_c} = \begin{cases} 1.03(\omega^*)^{1.425} & \text{for } 1 \leqslant \omega^* \leqslant 6 \\ 1.40(\omega^*)^{1.263} & \text{for } 6 \leqslant \omega^* \leqslant 110 \end{cases}$$
$$\frac{A}{A_c} = \begin{cases} 0.93(\omega^*)^{1.136} & \text{for } 1 \leqslant \omega^* \leqslant 6 \\ 0.94(\omega^*)^{1.146} & \text{for } 6 \leqslant \omega^* \leqslant 110 \end{cases} \tag{4}$$

where P_c and A_c are the contact load and real contact area at the inception of plastic deformation, respectively.

The second stage consists of the unloading process, where the interference, ω, is gradually reduced. When the unloading process is completed, the contact load, contact radius, and real contact area fall to zero. However, the original un-deformed spherical geometry is not fully recovered. Residual stresses and strains remain locked in, and result in a deformed shape of the unloaded sphere. This deformed shape is limited to a relatively narrow zone of the loaded contact prior to unloading and its immediate vicinity. The deformed profile of the unloaded sphere may be characterized by a residual interference ω_{res} and a residual non-uniform curvature with a radius R_{res} at its summit as shown schematically in Fig. 2. The residual interference ω_{res} and residual deformed profile with its summit residual curvature R_{res} depend on the loading level in terms of ω_{max} or P_{max} from which the unloading process started.

For a relatively moderate loading, the residual radius R_{res} may be evaluated analytically using the approach suggested by Johnson (1985). Assuming a reversible unloading process, a subsequent loading to ω_{max} will obey the elastic Hertz solution for a perfect spherical shape with a uniform radius R_{res} and a new interference $\omega = \omega_{max} - \omega_{res}$. The final contact load and contact radius upon completion of the reloading will be P_{max} and a_{max} respectively. According to the elastic contact Hertz theory (see e.g. Johnson, 1985 or Timoshenko and Goodier, 1970) the contact radius a is related to the interference, ω, and the sphere radius, R by

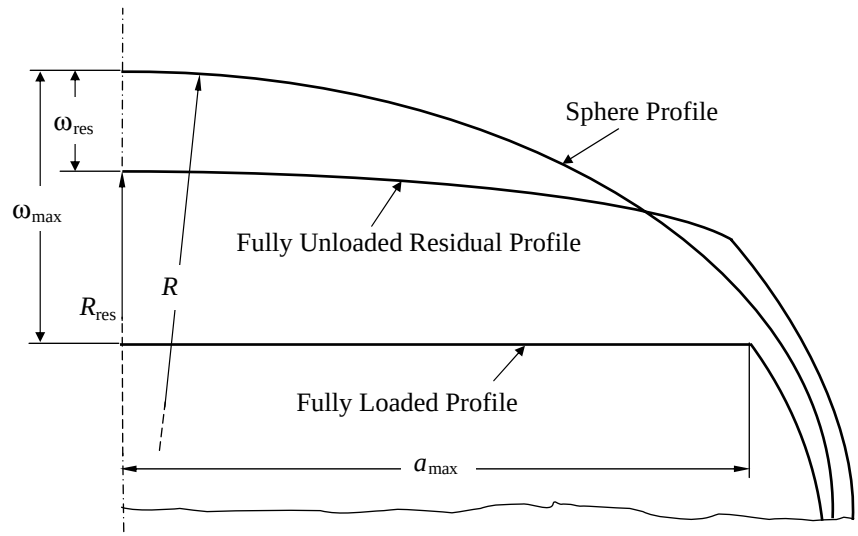

Fig. 2. Three different elastic–plastic stages of the unloading problem.

$$a = \sqrt{\omega R} \tag{5}$$

From geometrical considerations, the axial displacement of a given contacting point on the spherical surface, having a radial coordinate r, is:

$$u_z = \omega - \frac{r^2}{2R} \quad (r \leqslant a) \tag{6}$$

This displacement is related to the maximum pressure, p_0, in the center of the contact zone by:

$$u_z = \frac{1}{E^*}\frac{\pi p_0}{4a}(2a^2 - r^2) \tag{7}$$

The total load, P, compressing the two solids is given by

$$P = \int_0^a p(r) 2\pi r \, \mathrm{d}r = \frac{2}{3} p_0 \pi a^2 \tag{8}$$

For the subsequent loading of the unloaded spherical shape from ω_{res} to ω_{max} Eq. (5) yields:

$$a_{max} = \sqrt{(\omega_{max} - \omega_{res}) R_{res}} \tag{9}$$

From Eqs. (6) and (7) it follows that:

$$\frac{1}{E^*}\frac{\pi p_0}{4a_{max}}(2a_{max}^2 - r^2) = (\omega_{max} - \omega_{res}) - \frac{r^2}{2R} \tag{10}$$

Hence, for $r = 0$ Eq. (10) leads to:

$$\frac{1}{E^*}\frac{\pi p_0 a_{max}}{2} = \omega_{max} - \omega_{res} \tag{11}$$

Finding p_0 from Eq. (8) for P_{max} and a_{max} and substituting in Eq. (11) the residual interference ω_{res} can be expressed in the form

$$\frac{\omega_{res}}{\omega_{max}} = 1 - \frac{3P_{max}}{4E^* a_{max}\omega_{max}} \tag{12}$$

Substituting in Eq. (11) p_0 from Eq. (8) and $(\omega_{max} - \omega_{res})$ from Eq. (9) leads to a simple relation between the residual radius R_{res} and the initial contact load, P_{max}, prior to unloading, in the form:

$$R_{res} = \frac{4E^*}{3}\frac{a_{max}^3}{P_{max}} \tag{13}$$

The residual radius of Eq. (13) can also be expressed in terms of the initial mean contact pressure p_{max} before unloading,

$$R_{res} = \frac{4}{3}\frac{Ea_{max}}{\pi p_{max}(1 - \nu^2)} \tag{13a}$$

A similar expression but with a constant of 2/3 instead of 4/3 is presented in Majumder et al. (2003) for the residual radius in an unloaded MEMS microswitch.

3. The finite elements model

A commercial ANSYS 8.0 package was used to solve the load–unload contact problem. The model shown in Fig. 1 had a finite element mesh that consisted of 1920 six-node triangular elements comprising

Table 1
Materials and geometrical properties combinations

Case	Symbol	E, GPa	σ_y, MPa	v	R, mm	ω_c, μm	E/σ_y	ω_c/R
1	◊	200	210	0.32	10	0.0590	952.4	5.90×10^{-6}
2	+	80	220	0.30	2	0.0810	363.6	40.5×10^{-6}
3	○	69	28	0.30	10	0.0088	2464.3	0.88×10^{-6}
4	×	80	220	0.30	1	0.0403	363.6	40.3×10^{-6}
5	□	106	357	0.31	10	0.6053	296.9	60.5×10^{-6}
6	△	100	105	0.32	10	0.0590	952.4	5.90×10^{-6}

a total of 3987 nodes. The sphere was divided into four different mesh density zones where zones I, II, and III were within $0.01R$, $0.05R$, and $0.1R$ distance, respectively, from the sphere tip and zone IV, outside the $0.1R$ distance. Zone I had the finest mesh and all zones had gradual coarser mesh at increasing distance from the sphere tip. The material of the sphere was modeled as an elastic linear hardening material. A 2% linear hardening was selected since it still yields results that are very close to an elastic–perfectly plastic case, thus enabling comparison with existing loading results of Kogut and Etsion (2002), yet providing a much better convergence of the numerical solution. The von Mises yielding criterion was used to detect local transition from elastic to plastic deformation, and the Prandtl–Reuss constitutive law governed the stress–strain state in the plastic zones.

Different materials and hemispherical radii were analyzed (see Table 1) to study the effect of these variables on the elastic–plastic contact loading–unloading behavior. These parameters were selected in such a way that the critical interference, ω_c, which seems to be the most characteristic parameter of elastic–plastic contact problems, varied over a wide range of values from about 0.0088 μm to 0.605 μm. The ratio of E/σ_y also covered a wide range from about 297 to 2464. Also shown in Table 1 is the ratio ω_c/R which is uniquely determined by E/σ_y through Eq. (1) and the relation between H and σ_y. The hemisphere was loaded to various contact interference values with an upper limit of $\omega^* = 170$. Loading beyond this value is outside the scope of the present study. It requires the treatment of very large deformations that may be relevant in plastic forming.

In all the numerical simulations that were performed with the perfect slip condition at the contact, it was found that during the loading stage the radial displacements of the contacting points are negligibly small compared to their corresponding axial displacements. This suggests that in general there may be a very little tendency to slip at the contact interface, and hence, the assumption of perfect slip condition at the contact may not restrict the generality of the solution.

4. Discussion of the numerical results

Fig. 3 presents the dimensionless elastic–plastic load–displacement results for the loading–unloading process in terms of P^* vs. ω^*, while Fig. 4 presents the corresponding dimensionless results for the contact area A^*. The figures demonstrate results for three very different cases (cases 1, 2 and 5 in Table 1) in terms of E/σ_y ratio, sphere radius and ω_c. As can be seen from Figs. 3 and 4 scaling the variables with their corresponding critical values at plastic yield inception renders the dimensionless solution a universal nature that is independent of the physical and geometrical properties of the sphere. The dashed line in Fig. 3 presents the elastic–plastic loading results obtained by Kogut and Etsion (2002) for an elastic–perfectly plastic material (Eq. (4) above). As can be seen these results correlate well with the present model. The contact area results of Eq. (4) are identical to the present model loading results shown in Fig. 4. A best fit of the current numerical results for the elastic–plastic loading over the range of ω^* values up to 170 is presented by the solid lines in Figs. 3 and 4, and by the following empirical relations:

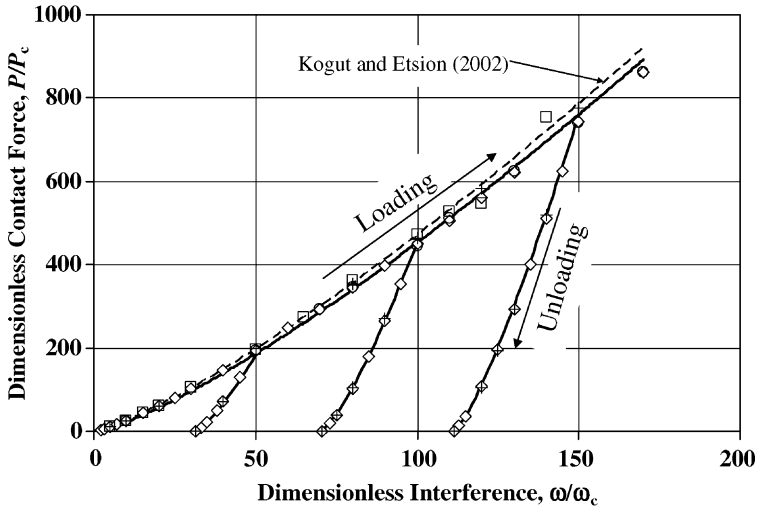

Fig. 3. Dimensionless contact load vs. dimensionless interference.

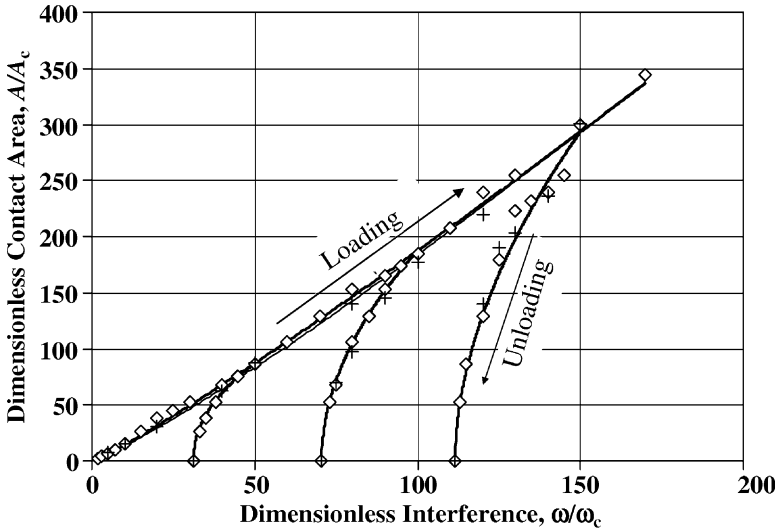

Fig. 4. Dimensionless contact area vs. dimensionless interference.

$$P^* = 1.32(\omega^* - 1)^{1.27} + 1$$
$$A^* = 1.19(\omega^* - 1)^{1.1} + 1 \tag{14}$$

Note that Eq. (14) are somewhat simpler than Eq. (4) since they provide a single expression that covers a wide range of ω^* values without the need to divide the range at $\omega^* = 6$ into two different expressions. This simplicity however, has its cost in accuracy and whereas Eq. (4) have an error of no more than 3% compared to the FEA numerical results, the error found in Eq. (14) can reach 16% in P^* and 18% in A^* at $\omega^* = 2$. The errors involved with Eq. (14) gradually decrease with increasing ω^* and for $\omega^* > 100$ the maximum error involved in using Eq. (14) is only about 3%.

The numerical results of the unloading process initiated from three representative ω^*_{max} values of 50, 100, and 150, respectively, are also shown in Figs. 3 and 4 for the cases 1, 2 and 5 of Table 1. It seems from these results that the present dimensionless solution is universal not only for the loading but also for the unloading stage. It is also clear from Fig. 3 that the load–displacement behavior during unloading is not linear and is strongly affected by the level of initial loading ω^*_{max}. The residual interference ω^*_{res} for any given initial value of ω^*_{max} can be found from the unloading process at its completion when the contact load vanishes. A best fit that was carried out on many unloading cases from various initial ω^*_{max} values (see also Fig. 5) resulted in a useful empirical relation for $\omega_{res}/\omega_{max}$ in the form:

$$\frac{\omega_{res}}{\omega_{max}} = \left(1 - \frac{1}{(\omega_{max}/\omega_c)^{0.28}}\right)\left(1 - \frac{1}{(\omega_{max}/\omega_c)^{0.69}}\right) \tag{15}$$

Similarly, from many unloading numerical results like the typical ones shown in Figs. 3 and 4 the following empirical relations were found for the load–displacement behavior and for the contact area, respectively during unloading:

$$\begin{aligned} P^* &= \frac{P}{P_c} = P^*_{max}\left(\frac{\omega^* - \omega^*_{res}}{\omega^*_{max} - \omega^*_{res}}\right)^{n_p} \\ A^* &= \frac{A}{A_c} = A^*_{max}\left(\frac{\omega^* - \omega^*_{res}}{\omega^*_{max} - \omega^*_{res}}\right)^{n_a} \end{aligned} \tag{16}$$

where

$$\begin{aligned} n_p &= 1.5(\omega^*_{max})^{-0.0331} \\ n_a &= (\omega^*_{max})^{-0.12} \end{aligned} \tag{17}$$

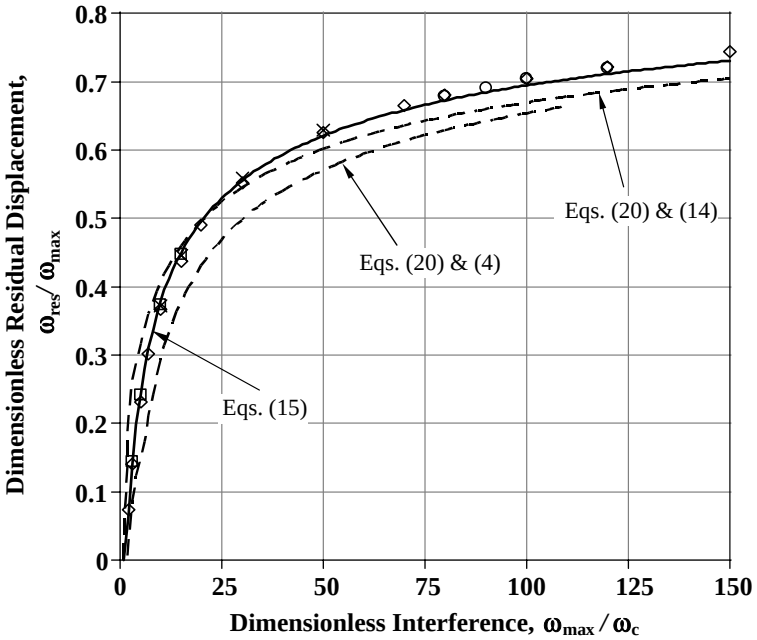

Fig. 5. Dimensionless residual interference vs. dimensionless maximum interference.

Hence, by using Eqs. (15) and (17) together with the proper relations in Eq. (4) or (14) for the maximum loading $\omega^* = \omega^*_{max}$ in Eq. (16), it becomes obvious that ω^*_{max} is indeed the major parameter affecting both the contact load and contact area behavior during the unloading process.

Fig. 5 presents the numerical results from which the relation of Eq. (15) (which is also presented in the figure by the solid line) was derived. As can be seen the residual interference ω_{res} decreases with a decreasing level of the initial elastic–plastic loading and it completely vanishes for pure elastic loading when $\omega^*_{max} \leqslant 1$. On the other hand, as the level of elastic–plastic loading increases, the residual interference approaches asymptotically an upper limit. This upper limit, which is ω_{max}, is obtained at very large initial plastic deformations when the elastic recovery becomes negligibly small compared to the initial ω_{max}.

The behavior of the residual interference discussed above is very well depicted in Eq. (15) for the extreme cases of $\omega_{max} = \omega_c$ and $\omega_{max} \to \infty$. In the first case Eq. (16) becomes:

$$P^* = (\omega^*)^{\frac{3}{2}} \tag{18}$$

describing a purely elastic nonlinear force–displacement unloading process that follows the loading Hertz solution. In the second case the force–displacement behavior during unloading (see Fig. 3) degenerates to:

$$\omega^* = \omega^*_{res} = \omega^*_{max} \tag{19}$$

which describes a purely plastic unloading process. It should be noted here that although the first load–unload cycle may be non-elastic, the first unloading can be fully reversible upon subsequent loading. Indeed, a few second loading processes that were performed on the present model for several ω^*_{max} values up to 150 indicated such fully reversible behavior. This suggests that following the first load–unload cycle all subsequent cycles of load–unload will be fully elastic. A full study of the multiple loading problem is outside the scope of the present paper and will be dealt with in a separate one.

It seems that the dimensionless residual interference, ω^*_{res}, can be used as a measure of the plasticity level of the loaded sphere. We shall term this ω^*_{res} an "elastic–plastic loading (EPL) index" that varies between 0 and 1 where the lower and upper limits correspond to purely elastic and purely plastic loading conditions, respectively. An almost identical measure of the plasticity level of the loaded sphere was obtained from a more elaborate energetic approach by finding the ratio between the dissipated energy due to plastic deformations and the work done to deform the sphere during loading (see Fig. 3).

$$EPL_E = \frac{\int_0^{\omega_{max}} P_L \, d\omega - \int_{\omega_{res}}^{\omega_{max}} P_{UL} \, d\omega}{\int_0^{\omega_{max}} P_L \, d\omega}$$

where the subscripts L and UL correspond to the loading and unloading, respectively. In case where the contact load during loading and unloading varies linearly with the displacement (which is a fair approximation as can be seen from Fig. 3) the above energetic approach yields exactly ω^*_{res}.

The EPL index differs from the well known GW plasticity index, ψ, for rough surfaces (Greenwood and Williamson, 1966) in that the latter depends on ω_c and on surface topography but is totally insensitive to the contact loading. The EPL index, on the other hand, strongly depends (in addition to ω_c) on the loading level through ω_{max}. It therefore better indicates the plasticity level of individual asperities and may lead to a more physical "plasticity index" of contacting rough surfaces by considering their unloading from any elastic–plastic loading level.

Note that the discrete numerical results shown in Fig. 5 were obtained for all the different cases of the sphere material and geometrical properties combinations shown in Table 1. It is very clear from the figure that the dimensionless residual interference, $\omega_{res}/\omega_{max}$, and, hence, the EPL index is independent of these physical and geometrical properties. This, once again, demonstrates the powerful universality of the present model.

The dashed lines shown in Fig. 5 represent the analytical relation of Eq. (12). It was obtained by using the Hertz solution for the relation $P_c = (4/3)E^* a_c \omega_c$, which upon substituting in Eq. (12) yields

$$\frac{\omega_{res}}{\omega_{max}} = 1 - \frac{P_{max}/P_c}{(a_{max}/a_c)(\omega_{max}/\omega_c)} \tag{20}$$

Noting that $a_{max}/a_c = (A_{max}/A_c)^{0.5}$ and using Eq. (4) or (14) the right-hand side of Eq. (20) becomes a function of ω_{max}/ω_c only. As can be seen from Fig. 5 the analytical approach of Johnson (1985) fairly approximates the numerical results.

Fig. 6 presents the numerical results of the residual radius of curvature, R_{res}, at the summit of the deformed fully unloaded sphere (see Fig. 2), normalized by the uniform radius R of the un-deformed original sphere vs. the initial loading level in terms of ω^*_{max}. All the six cases of Table 1 are represented and it is clear from the figure that they depend on the ratio E/σ_y The numerical results are well fitted by the expression:

$$R_{res}/R = 1 + 1.275\left(\frac{E}{\sigma_y}\right)^{-0.216} \qquad (\omega_{max}/\omega_c - 1) \tag{21}$$

The dashed lines in Fig. 6 were obtained from Eq. (13) by using the Hertzian relation $P_c = (4/3)E^*(a_c^3/R)$. This resulted in:

$$\frac{R_{res}}{R} = \frac{(a_{max}/a_c)^3}{P_{max}/P_c} \tag{22}$$

this, again, by using Eq. (4) or (14), can be expressed in terms of ω_{max}/ω_c only. As can be seen from Fig. 6 Eq. (22) or (13), which was obtained analytically by assuming pure elastic unloading, is indeed valid only for low elastic–plastic loading levels but largely underestimates the residual radius R_{res} over most of the elastic–plastic loading range. Recall that a major assumption made in developing Eqs. (13) and (22) was that the unloaded sphere maintains a perfect spherical shape with a uniform radius of curvature R_{res} somewhat larger than the original radius R. This assumption was examined in the present study by finding the distribution of local residual curvature of the free surface of the unloaded sphere as a function of the radial

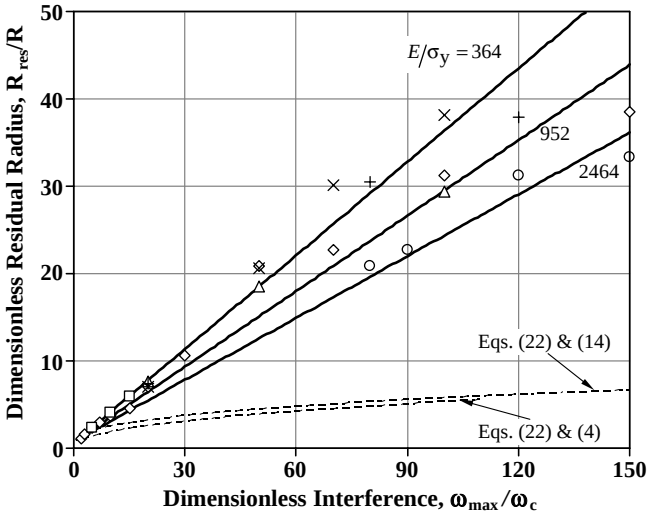

Fig. 6. Dimensionless residual tip radius of curvature vs. dimensionless maximum interference.

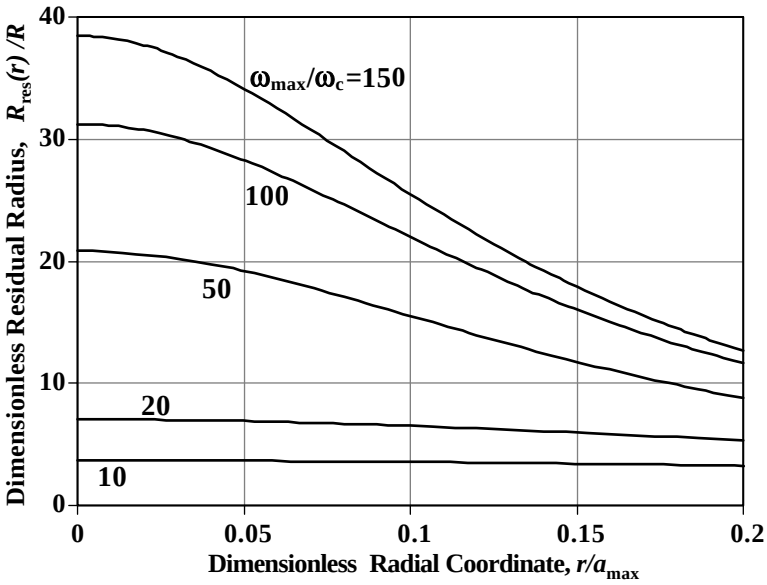

Fig. 7. Dimensionless local residual radius of curvature vs. dimensionless radial coordinate.

coordinate r. This was accomplished by curve fitting the numerical results of the sphere surface nodes position after unloading and then finding analytically the local curvature of the obtained curve.

Fig. 7 presents the results of the normalized local residual curvature as a function of the normalized radial coordinate, r/a_{max}, for several elastic–plastic loading levels, ω^*_{max}. The results shown are limited to $r/a_{max} < 0.2$ namely, to a small central portion of the formerly loaded contact area. As can be seen from Fig. 7 the residual radius of curvature, R_{res}, at the summit of the unloaded sphere, can be much larger

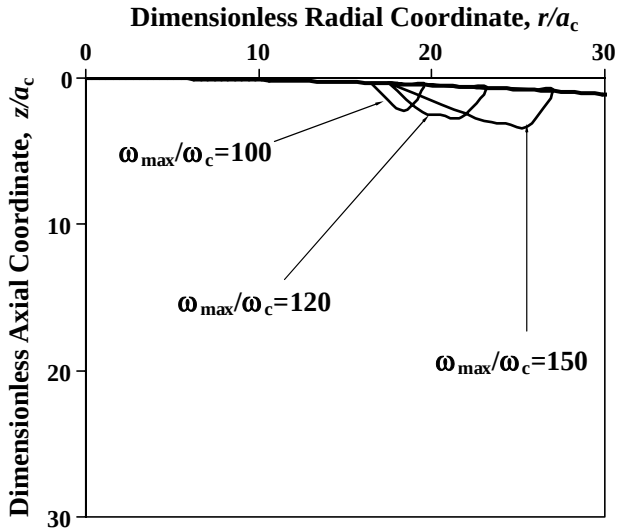

Fig. 8. Plastic regions at full unloading from three levels of relatively high elastic–plastic loading.

than the original un-deformed sphere radius, up to 40 times larger at the highest loading level. At larger r/a_{max} value the normalized local residual curvature decreases and eventually may approach unity far enough from the initial contact zone. As evident from the figure, the residual radius of curvature remains uniform over the 20% range of a_{max} only for modest loadings with $\omega^*_{max} \leqslant 20$ and even then it is from 5 to 8 times larger than the original sphere radius. At higher loading level the local residual curvature distribution in the vicinity of the unloaded sphere summit is highly non-uniform. At $\omega_{max}/\omega_c = 50$, for example, the variation over a dimensionless radial span of 0.2 is about 100%, hence, very different from the simplified approach of Johnson (1985).

Finally it is interesting to find out if any plastic zones remain locked inside the sphere upon completion of the unloading process. Fig. 8 presents contours of such plastic zones that were found only when the unloading started from higher levels of loading in terms of ω_{max}/ω_c. As can be seen from the figure these plastic zones are formed during the unloading process around the circumference of the loaded contact area while the plastic zones that formed during the loading process under this contact area (see Kogut and Etsion, 2002) disappear.

5. Conclusion

The unloading of an elastic–plastic spherical contact loaded by a rigid flat was analyzed by FEA for a large range of material and geometrical properties of the loaded sphere. Analytical expressions for the dimensionless contact load and contact area vs. displacement during unloading, and for the residual radius of curvature and residual interference at the end of the unloading process, were derived by best fitting of the numerical FEA results. A wide range of loading levels in terms of the maximum contact interference was covered and the dimensionless model was found to be universal in nature and independent of specific material or radius of the sphere. An elastic–plastic loading index (EPL index) was suggested, based on the dimensionless residual interference, which may serve as a measure of the level of plasticity of the loaded sphere. The main conclusion of the present analysis is that whereas the first load–unload cycle of a spherical contact can be a non-linear and non-elastic phenomenon, the first unloading can be fully reversible and subsequent multiple load–unload cycles can be elastic. More in depth study of multiple loading–unloading is required.

Acknowledgment

This research was partially supported by The Israel Science Foundation.

References

Chang, W.R., Etsion, I., Bogy, D.B., 1987. An elastic–plastic model for the contact of rough surfaces. ASME J. Tribol. 109, 257–263.

Chang, W.R., Etsion, I., Bogy, D.B., 1988. Adhesion model for metallic rough surfaces. ASME J. Tribol. 110, 50–56.

Greenwood, J.A., Williamson, J.B.P., 1966. Contact of nominally flat surfaces. Proc. Roy. Soc., Lond. A 295, 300–319.

Johnson, K.L., 1985. Contact Mechanics. Cambridge University Press, Cambridge, MA.

Kim, J.-Y., Baltazar, A., Rokhlin, S.I., 2004. Ultrasonic assessment of rough surface contact between solids from elastoplastic loading–unloading hysteresis cycle. J. Mech. Phys. Solids 52 (8), 1911–1934.

Kogut, L., Etsion, I., 2002. Elastic–plastic contact analysis of a sphere and a rigid flat. ASME J. Appl. Mech. 69, 657–662.

Li, L.-Y., Wu, C.-Y., Thornton, C., 2002. A theoretical model for the contact of elastoplastic bodies. Proc. Instn. Mech. Engrs. 216 (Part C), 421–431.

Lin, Y.Y., Hui, C.Y., 2002. Mechanics of contact and adhesion between viscoelastic spheres: an analysis of hysteresis during loading and unloading. J. Polymer Sci. Part B—Polymer Phys. 40 (9), 772–793.

Majumder, S., McGruer, N.E., Adams, G.G., Zavracky, A.P., Zavracky, P.M., Morrison, R.H., Krim, J., 2001. Study of contacts in an electrostatically actuated microswitch. Sensors Actuators A 93, 19–26.

Majumder, S., McGruer, N.E., Adams, G.G., 2003. Contact resistance and adhesion in a MEMS microswitch. In: Proc. of 2003 STLE/ASME Joint Int. Tribol. Conf. 2003-TRIB-270. pp. 1–6.

Mesarovic, S.D., Johnson, K.L., 2000. Adhesive contact of elastic–plastic spheres. J. Mech. Phys. Solids 48 (10), 2009–2033.

Peng, W., Bhushan, B., 2003. Transient analysis of sliding contact of layered elastic/plastic solids with rough surfaces. Microsyst. Technol. 9 (5), 340–345.

Tabor, D., 1948. A simple theory of static and dynamic hardness. Proc. Roy. Soc., Lond. A 192, 247–274.

Tabor, D., 1951. The Hardness of Metals. Clarendon Press, Oxford, UK.

Timoshenko, S.P., Goodier, J.N., 1970. Theory of Elasticity, third ed. McGraw-Hill, New York.

Vu-Quoc, L., Zhang, X., Lesberg, L., 2000. A normal force–displacement model for contacting spheres accounting for plastic deformation: force-driven formulation. ASME J. Appl. Mech. 67 (2), 363–371.

Yan, S.L., Li, L.Y., 2003. Finite element analysis of cyclic indentation of an elastic–perfectly plastic half-space by a rigid sphere. Proc. Instn. Mech. Engrs., Part C: J. Mech. Eng. Sci. 217 (5), 505–514.

Ye, N., Komvopoulos, K., 2003. Effect of residual stress in surface layer on contact deformation of elastic–plastic layered media. ASME J. Tribol. 125 (4), 692–699.